

Production cross sections of neutron-rich $^{261-263}\text{No}$ isotopes

Jingjing Li,^{1,2} Cheng Li,^{1,2} Gen Zhang,^{1,2} Long Zhu,³ Zhong Liu,⁴ and Feng-Shou Zhang^{1,2,5,*}

¹The Key Laboratory of Beam Technology and Material Modification of Ministry of Education, College of Nuclear Science and Technology, Beijing Normal University, Beijing 100875, China

²Beijing Radiation Center, Beijing 100875, China

³Sino-French Institute of Nuclear Engineering and Technology, Sun Yat-sen University, Zhuhai 519082, China

⁴Institute of Modern Physics, Chinese Academy of Sciences, Lanzhou 730000, China

⁵Center of Theoretical Nuclear Physics, National Laboratory of Heavy Ion Accelerator of Lanzhou, Lanzhou 730000, China

(Received 28 February 2017; published 15 May 2017)

The fusion excitation functions of $^{249-263}\text{No}$ are studied by using various reaction systems based on the dinuclear system model. The neutron-rich radioactive beam ^{22}O is used to produce neutron-rich nobelium isotopes, and the new neutron-rich isotopes $^{261-263}\text{No}$ are synthesized by $^{242}\text{Pu}(^{22}\text{O},3n)^{261}\text{No}$, $^{244}\text{Pu}(^{22}\text{O},4n)^{262}\text{No}$, and $^{244}\text{Pu}(^{22}\text{O},3n)^{263}\text{No}$ reactions, respectively. The corresponding maximum evaporation residue cross sections are 0.628, 4.649, and 1.638 μb , respectively. The effects of the three processes (capture, fusion, and survival) in the complete fusion reaction are also analyzed. From investigation, a neutron-rich radioactive beam as the projectile and neutron-rich actinide as the target could be a new selection of the projectile-target combination to produce a neutron-rich heavy nuclide.

DOI: 10.1103/PhysRevC.95.054612

I. INTRODUCTION

The fusion-evaporation (FE) reaction is an effective method to produce heavy and superheavy elements (SHEs). Great progress in the synthesis of new heavy and superheavy nuclei by fusion reactions has been made in recent years; for instance, $^{281-285}\text{Cn}$, $^{282-286}\text{Nh}$, $^{285-289}\text{Fl}$, $^{287-290}\text{Mc}$, $^{290-293}\text{Lv}$, $^{293,294}\text{Ts}$, and ^{295}Og have been synthesized by using ^{48}Ca beams and actinide targets from ^{238}U to ^{249}Cf during the past 15 years [1–8]. However, due to the limitation of the neutron number of stable projectiles and targets, among the elements with $Z > 100$ only neutron-deficient isotopes have been produced. The effort to reach the nuclear landscape in the region of $Z > 100$ toward the neutron drop-line has been attracting wide attention currently. The element nobelium ($Z = 102$) was discovered by Donets *et al.* and Zager *et al.* with the reactions $^{243}\text{Am}(^{15}\text{N},4n)^{254}\text{No}$ and $^{238}\text{U}(^{22}\text{Ne},6n)^{254}\text{No}$ in 1965 [9,10]. Up to now, only 11 isotopes ($^{250-260}\text{No}$) have been produced [9–18]. The synthesis methods of nobelium isotopes are summarized in Table I. ^{260}No was the only isotope obtained by using the multinucleon transfer (MNT) reaction, the rest were synthesized by using the FE reaction. Therefore, the research of No isotopes with $A \geq 261$ has attracted great attention and interest [19].

Experimental research has shown that fusion cross sections are enhanced in reactions of neutron-rich ^{38}S on ^{181}Ta [20] and ^{208}Pb [21] and ^{132}Sn on ^{64}Ni [22]. The neutron-rich system leads to the lowering of the barrier height which enhances the fusion cross section. Today radioactive ion beam facilities can provide very neutron-rich projectiles, such as ^{8-11}Li , $^{10,11}\text{Be}$, $^{14-16}\text{C}$, $^{16-18}\text{N}$, $^{19-22}\text{O}$, $^{20-23}\text{F}$, $^{23-26}\text{Ne}$, and $^{24-31}\text{Na}$. We expect that new neutron-rich nuclei could be produced by using fusion reactions with radioactive beams. However the

interaction mechanism of fusion reactions between neutron-rich projectiles and targets in capture, fusion, and survival processes is unclear.

Many theories have been proposed to describe the heavy-ion fusion process. The microscopic dynamics models, such as the improved quantum molecular dynamics model [23] and the time-dependent Hartree-Fock model [24], have shown reasonable success in the description of neck formation, which derives from the nucleon transfer and the dynamical deformation under the effective mean-field potentials [23,24]. The semiclassical models, such as the two-step model [25], the dinuclear system (DNS) model [26], the fusion-by-diffusion model [27,28], and some others [29–32], have achieved remarkable success in describing the evaporation residual cross sections of superheavy nuclei. The aim of this work is to synthesize more neutron-rich nobelium isotopes by using the FE reaction within the DNS model. The capture, fusion, and survival mechanisms in the fusion process are analyzed via $^{18}\text{O} + ^{244}\text{Pu}$ and $^{22}\text{O} + ^{244}\text{Pu}$ reactions. Then the evaporation residue cross sections of $^{48}\text{Ca} + ^{208}\text{Pb}$, $^{26}\text{Mg} + ^{228,230}\text{Th}$, $^{18}\text{O} + ^{242,244}\text{Pu}$, and $^{22}\text{O} + ^{242,244}\text{Pu}$ systems are systematically studied in the DNS framework.

The paper is organized as follows. In Sec. II, we briefly introduce the DNS model. In Sec. III, the production cross sections of nobelium isotopes in different reactions are calculated. Finally, we give the conclusions in Sec. IV.

II. THE MODEL

In the DNS framework, the evaporation residue cross section in heavy-ion fusion reactions is calculated [33] as follows:

$$\sigma_{\text{ER}}(E_{\text{c.m.}}) = \frac{\pi \hbar^2}{2\mu E_{\text{c.m.}}} \sum_J (2J+1) T(E_{\text{c.m.}}, J) \times P_{\text{CN}}(E_{\text{c.m.}}, J) W_{\text{sur}}(E_{\text{c.m.}}, J), \quad (1)$$

*Corresponding author: fszhang@bnu.edu.cn

TABLE I. A brief summary of the No isotopes.

Reaction	$E_{\text{lab}}(\text{MeV})$	Method	Channel	Isotope	References
$^{48}\text{Ca} + ^{206}\text{Pb}$	213.5–242.5	FE	$4n$	^{250}No	[11]
$^{48}\text{Ca} + ^{204}\text{Pb}$	213.5–242.5	FE	$2n$	^{250}No	[11]
$^{12}\text{C} + ^{244}\text{Cm}$	78 – 90	FE	$5n$	^{251}No	[12]
$^{18}\text{O} + ^{239}\text{Pu}$	96	FE	$5n$	^{252}No	[13]
$^{16}\text{O} + ^{242}\text{Pu}$	102	FE	$5n$	^{253}No	[13]
$^{22}\text{Ne} + ^{238}\text{U}$	—	FE	$6n$	^{254}No	[9]
$^{15}\text{N} + ^{243}\text{Am}$	82–84	FE	$4n$	^{254}No	[9,10]
$^{22}\text{Ne} + ^{238}\text{U}$	177	FE	$5n$	^{255}No	[14]
$^{22}\text{Ne} + ^{238}\text{U}$	110–120	FE	$4n$	^{256}No	[15]
$^{13}\text{C} + ^{248}\text{Cm}$	63–68	FE	$4n$	^{257}No	[12]
$^{13}\text{C} + ^{248}\text{Cm}$	67.6	FE	$3n$	^{258}No	[16]
$^{18}\text{O} + ^{248}\text{Cm}$	88–106	FE	$\alpha 3n$	^{259}No	[17]
$^{18}\text{O} + ^{254}\text{Es}$	99	MNT	—	^{260}No	[18]

where T , P_{CN} , and W_{sur} are the transmission probability, the fusion probability, and the survival probability, respectively. The capture cross section $\sigma_{\text{cap}}(E_{\text{c.m.}}, J)$ is expressed as [26,34,35]

$$\sigma_{\text{cap}}(E_{\text{c.m.}}) = \frac{\pi \hbar^2}{2\mu E_{\text{c.m.}}} \sum_J (2J+1) T(E_{\text{c.m.}}, J). \quad (2)$$

The capture process is usually treated with an empirical coupled-channel model approach [29], in which the barrier distribution function method is introduced. Figure 1 shows the capture cross sections of $^{48}\text{Ca} + ^{208}\text{Pb}$ as a function of the excitation energy of the system. One can see that the calculated results are in good agreement with the experimental data.

The fusion probability is obtained by solving a set of master equations within the corresponding potential energy surface (PES) [36,37]. The distribution probability of fragments for the dinuclear system is calculated based on the following master

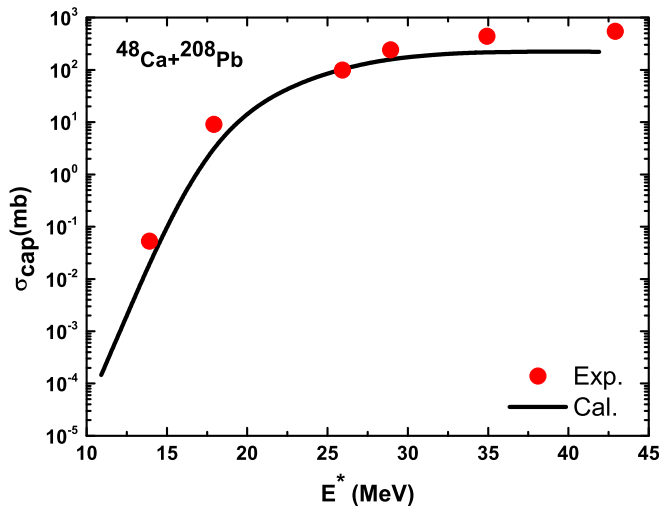


FIG. 1. The measured (circle) [11] and calculated (solid line) capture cross sections for the reaction $^{48}\text{Ca} + ^{208}\text{Pb}$ formed in the dinuclear system.

equation:

$$\begin{aligned} & \frac{dP(Z_1, N_1, E_1, t)}{dt} \\ &= \sum_{Z'_1} W_{Z_1, N_1; Z'_1, N'_1}(t) [d_{Z_1, N_1} P(Z'_1, N_1, E'_1, t) \\ & \quad - d_{Z'_1, N'_1} P(Z_1, N_1, E_1, t)] \\ & \quad + \sum_{N'_1} W_{Z_1, N_1; Z_1, N'_1}(t) [d_{Z_1, N_1} P(Z_1, N'_1, E'_1, t) \\ & \quad - d_{Z_1, N'_1} P(Z_1, N_1, E_1, t)] \\ & \quad - [\Lambda_{\text{qf}}(\Theta(t)) + \Lambda_{\text{fis}}(\Theta(t))] P(Z_1, N_1, E_1, t), \quad (3) \end{aligned}$$

where $P(Z_1, N_1, E_1, t)$ is the probability function at time t and excitation energy E_1 to get fragment 1 with proton number Z_1 and neutron number N_1 . $W_{Z_1, N_1; Z'_1, N'_1}$ is the mean transition probability from channel (Z_1, N_1, E_1) to (Z'_1, N'_1, E'_1) . d_{Z_1, N_1} denotes the microscopic dimensions corresponding to the macroscopic state (Z_1, N_1, E_1) . The sum is taken over all possible proton and neutron numbers that fragment Z'_1, N'_1 may take. Λ_{qf} and Λ_{fis} are the quasifission rate and fission rate, respectively, which could be estimated from a one-dimensional Kramers formula [38,39].

The PES of the DNS can be written as

$$\begin{aligned} U(Z_1, N_1, Z_2, N_2, R, \beta_1, \beta_2, J) \\ &= U_{LD}(Z_1, N_1) + U_{LD}(Z_2, N_2) - U_{LD}(Z, N) \\ & \quad - V_{\text{rot}}^{\text{CN}}(J) + V_N(Z_1, N_1, Z_2, N_2, R, \beta_1, \beta_2, J) \\ & \quad + V_C(Z_1, Z_2, R, \beta_1, \beta_2, J). \quad (4) \end{aligned}$$

Here $U(Z_1, N_1, Z_2, N_2, R, \beta_1, \beta_2, J)$ is the driving potential of the DNS. $U_{LD}(Z_1, N_1)$, $U_{LD}(Z_2, N_2)$, and $U_{LD}(Z, N)$ are the binding energies of two deformed nuclei and the compound nucleus (CN), respectively. The variable R is the relative distance between two fragments located at bottom of the potential pocket. β_1 and β_2 represent the quadrupole deformations of two fragments. $V_{\text{rot}}^{\text{CN}}$ is the rotation energy

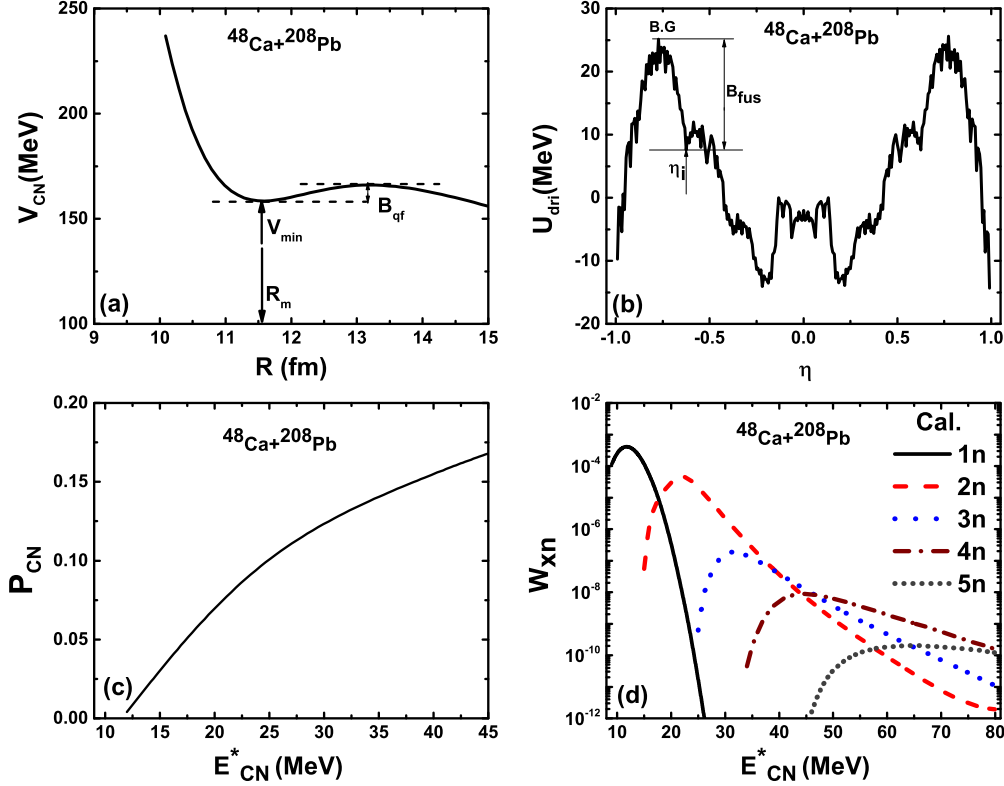


FIG. 2. (a) The interaction potentials in the entrance channel as a function of relative distance R for the reaction $^{48}\text{Ca} + ^{208}\text{Pb}$. (b) The driving potential for nucleon transfer in the reaction $^{48}\text{Ca} + ^{208}\text{Pb}$. The calculated (c) fusion probability and (d) survival probability as a function of E_{CN}^* .

of the compound nucleus. V_N and V_C are the nuclear potential and the Coulomb interaction, respectively, which are calculated by the double-folding method and Wong's formula [40,41].

Figure 2(a) shows the nucleus-nucleus interaction potential in the reaction $^{48}\text{Ca} + ^{208}\text{Pb}$. The DNS is formed when the potential well has the minimum value $V_{\text{min}} = 158.5$ MeV at $R_m = 11.59$ fm. The potential well depth B_{qf} is considered as the quasifission barrier, which is related to the decay of the DNS. For $^{48}\text{Ca} + ^{208}\text{Pb}$, $B_{\text{qf}} = 7.55$ MeV. The driving potential in the reaction $^{48}\text{Ca} + ^{208}\text{Pb}$ is presented in Fig. 2(b). The horizontal axis indicates the mass asymmetry expressed as $\eta = \frac{A_1 - A_2}{A_1 + A_2}$, and the vertical axis indicates the interaction potential. $\eta_i = -0.625$ represents the position of the mass asymmetry in the entrance channel. $B_{\text{fus}} = 17.56$ MeV is the inner fusion barrier, which supplies the important hindrance in the fusion process. Only enough energy is supplied to overcome the inner fusion barrier, the DNS could fuse to form the CN. The sum of the distribution probability that all the fragments pass over the Businaro Gallone (B.G.) point is defined as the fusion probability. Then the expression of the fusion probability is written as [41]

$$P_{\text{CN}}(E_{\text{c.m.}}, J) = \int f(B) P_{\text{CN}}(E_{\text{c.m.}}, J, B) dB, \quad (5)$$

and $P_{\text{CN}}(E_{\text{c.m.}}, J, B)$ is the formation probability of the CN with the barrier distribution function $f(B)$ and the angular

momentum J , which is given by

$$P_{\text{CN}}(E_{\text{c.m.}}, J, B) = \sum_{A_1=1}^{A_{\text{B.G.}}} P[A_1, E_1, \tau_{\text{int}}(E_{\text{c.m.}}, J, B)]. \quad (6)$$

Here $f(B)$ is taken as an asymmetric Gaussian form as described in Ref. [29]. $\tau_{\text{int}}(E_{\text{c.m.}}, J, B)$ is the interaction time, which is obtained by using the deflection function method [42]. Figure 2(c) shows the calculated fusion probability as a function of the excitation energy of the CN (E_{CN}^*) for the reaction $^{48}\text{Ca} + ^{208}\text{Pb}$. The fusion probability is small because of this system's small mass asymmetry.

Based on statistical model [43–45], the survival probability under the evaporation of x neutrons is written as [26]

$$W_{\text{sur}}(E_{\text{CN}}^*, x, J) = P(E_{\text{CN}}^*, x, J) \prod_{i=1}^x \left[\frac{\Gamma_n(E_i^*, J)}{\Gamma_n(E_i^*, J) + \Gamma_f(E_i^*, J)} \right], \quad (7)$$

where $P(E_{\text{CN}}^*, x, J)$ is the realization probability of the xn -evaporation channel with energy E_{CN}^* and angular momentum J . Γ_n and Γ_f are the widths of the neutron emission and fission, which are given by Weisskopf's evaporation theory [46] and the equation of Bohr-Wheeler [47]. For the details of the calculation of E_i^* and $P(E_{\text{CN}}^*, x, J)$, see Refs. [48–50].

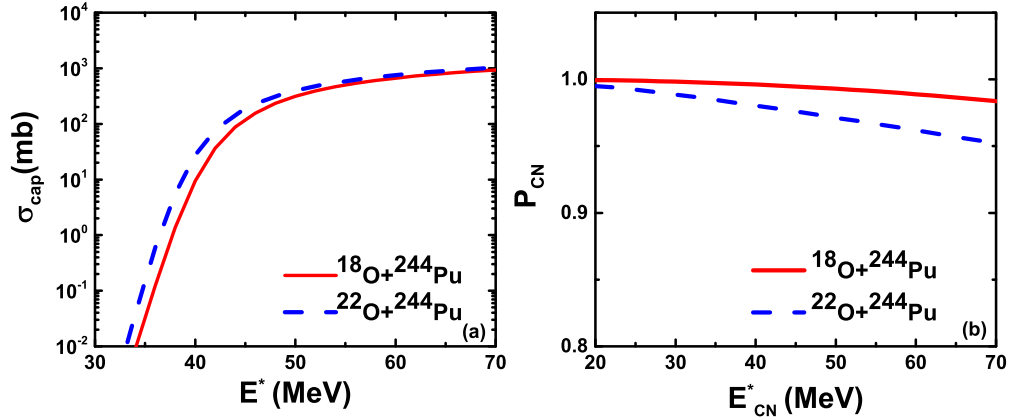


FIG. 3. The calculated (a) capture cross sections and (b) fusion probabilities for the reactions $^{18}\text{O} + ^{244}\text{Pu}$ and $^{22}\text{O} + ^{244}\text{Pu}$.

The calculated survival probability as a function of E_{CN}^* for the reaction $^{48}\text{Ca} + ^{208}\text{Pb}$ is shown in Fig. 2(d). The survival probabilities in the $1n$ and $2n$ emission channels are much larger than those in the $3n$, $4n$, and $5n$ emission channels.

III. RESULTS AND DISCUSSION

A. Three processes in the complete fusion reaction

Within the DNS model, the whole process of the compound nucleus formation and decay is divided into three individual stages, which are capture, fusion, and survival.

Figure 3(a) shows the capture cross sections of $^{18}\text{O} + ^{244}\text{Pu}$ and $^{22}\text{O} + ^{244}\text{Pu}$ as a function of excitation energy. The values of $V_b + Q$ for the $^{18}\text{O} + ^{244}\text{Pu}$ and $^{22}\text{O} + ^{244}\text{Pu}$ systems are 42.26 and 40.78 MeV, respectively. With the increasing of the excitation energy, the capture cross sections increase rapidly at excitation energies lower than $V_b + Q$. In this case, the capture process of the projectile and the target are dominated by the quantum tunneling effect. At E^* larger than $V_b + Q$, the increase of capture cross sections is due to the contribution

of the partial wave of the larger angular momentum. It can be seen that the capture cross section for the reaction $^{18}\text{O} + ^{244}\text{Pu}$ is lower than that for the reaction $^{22}\text{O} + ^{244}\text{Pu}$. This is because the reaction $^{22}\text{O} + ^{244}\text{Pu}$ has a lower $V_b + Q$ value.

The fusion probabilities of $^{18}\text{O} + ^{244}\text{Pu}$ and $^{22}\text{O} + ^{244}\text{Pu}$ as a function of E_{CN}^* are shown in Fig. 3(b). One can find that the fusion probability for $^{18}\text{O} + ^{244}\text{Pu}$ and $^{22}\text{O} + ^{244}\text{Pu}$ are in the interval 0.9–1.0 at E_{CN}^* from 20 to 70 MeV. In the fusion process, the quasifission probability increases with the enhancing of E_{CN}^* due to the decreasing of the quasifission barrier height. Hence, the fusion probabilities for these two systems slightly decrease as E_{CN}^* grows. In addition, the fusion probability of $^{18}\text{O} + ^{244}\text{Pu}$ is larger than that of $^{22}\text{O} + ^{244}\text{Pu}$ due to the system's larger mass asymmetry.

Figure 4 shows the survival probabilities of $^{18}\text{O} + ^{244}\text{Pu}$ and $^{22}\text{O} + ^{244}\text{Pu}$ under the evaporation of three to five neutrons. Because each neutron emission takes away about 8–10 MeV energy, one can see that the interval of peaks is about 10 MeV. The peak values decrease rapidly with increasing neutron emission channel, which is because the fission becomes

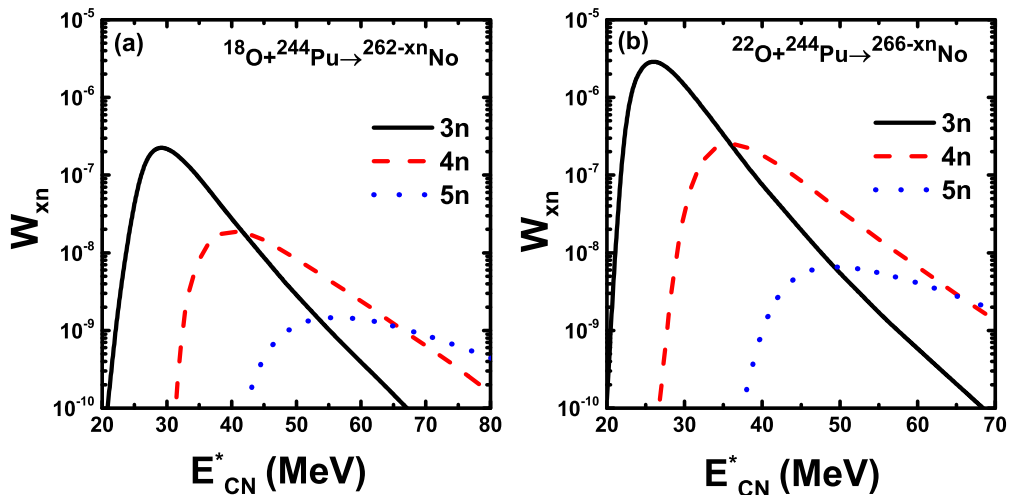


FIG. 4. The calculated survival probabilities as a function of E_{CN}^* under the evaporation of three to five neutrons for the reactions (a) $^{18}\text{O} + ^{244}\text{Pu}$ and (b) $^{22}\text{O} + ^{244}\text{Pu}$. The calculated results of the $3n$, $4n$, and $5n$ channels are indicated by solid, dashed, and dotted lines, respectively.

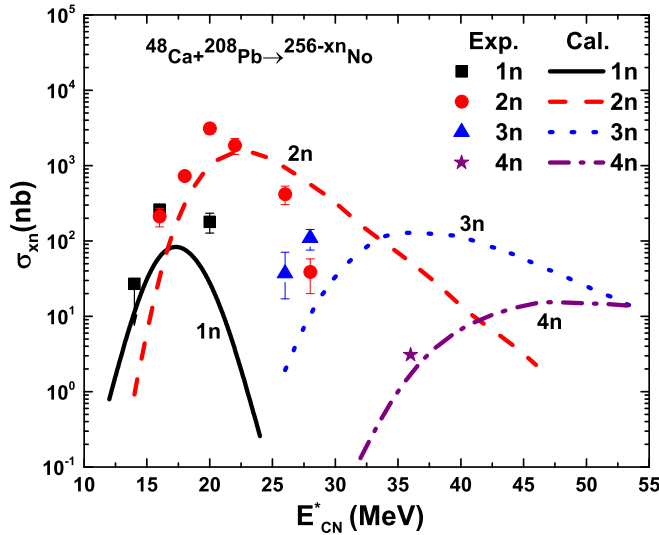


FIG. 5. The excitation functions in the xn -evaporation channels ($x = 1-4$) for the $^{48}\text{Ca} + ^{208}\text{Pb}$ reaction. The solid, dashed, dotted, and dash-dotted lines indicate calculated results of the $1n$, $2n$, $3n$, and $4n$ channels, respectively. The circles, squares, triangles, and pentagon represent the available experimental data [11] for the $1n$, $2n$, $3n$, and $4n$ channels, respectively.

more and more important at higher excitation energies. By comparing Figs. 4(a) and 4(b), we can see that the peak values of the $^{22}\text{O} + ^{244}\text{Pu}$ system are significantly larger than those of the $^{18}\text{O} + ^{244}\text{Pu}$ system in the corresponding neutron emission channel. This is because the CN with smaller neutrons usually has a lower fission barrier height and the fission width of the $^{18}\text{O} + ^{244}\text{Pu}$ system is larger than that of the $^{22}\text{O} + ^{244}\text{Pu}$ system at the same excitation energy.

B. Production cross sections of $^{249-263}\text{No}$

The excitation functions of $^{48}\text{Ca} + ^{208}\text{Pb}$ are presented in Fig. 5. The solid, dashed, dotted, and dash-dotted lines indicate the calculated results of the $1n$, $2n$, $3n$, and $4n$ channels, respectively. The circles, squares, triangles, and pentagon represent the available experimental data [11] for the $1n$, $2n$,

$3n$, and $4n$ channels, respectively. From Fig. 5, one can see that the calculated evaporation residue cross sections are in good agreement with the experimental data. The value of $V_b + Q$ for this system is 26 MeV, so E_{CN}^* lower than 26 MeV denotes that the reaction mechanism is dominated by subbarrier fusion. In this case, the capture section is lower, which leads to the peak value of σ_{1n} (94 nb), which is significantly lower than that of σ_{2n} (1604.7 nb). With excitation energy above 26 MeV, more neutrons will be emitted in the deexcitation process. Meanwhile, the fission channels become more and more important at high excited states; as a result, the calculated peak values of the $3n$ and $4n$ channels are rapidly decreased compared to that of the $2n$ channel. One can see that the maximum values of σ_{3n} and σ_{4n} reduce to 129 and 15 nb and the corresponding excitation energies are 36 and 45 MeV, respectively.

The evaporation residue cross sections in the reactions $^{26}\text{Mg} + ^{228}\text{Th}$ and $^{26}\text{Mg} + ^{230}\text{Th}$ are displayed in Fig. 6. The values of mass asymmetry of the $^{26}\text{Mg} + ^{228}\text{Th}$ and $^{26}\text{Mg} + ^{230}\text{Th}$ reaction systems are approximately 0.80. The values of $V_b + Q$ for these systems are 46.9 and 47.7 MeV, respectively. In the $^{26}\text{Mg} + ^{228}\text{Th}$ reaction, the maximum yields of the $3n$ and $4n$ channels are comparable at $E_{\text{CN}}^* = 47.0$ and 52.0 MeV. The maximum value of σ_{3n} (65.1 nb) is slightly larger than that of σ_{4n} (23.9 nb). In addition, neutron-deficient ^{249}No isotopes are produced with a maximum evaporation residue cross section of 1.2 nb in the $5n$ channel at $E_{\text{CN}}^* = 74.0$ MeV. In the $^{26}\text{Mg} + ^{230}\text{Th}$ reaction, the maximum values of $3n$ and $4n$ are almost the same (≈ 170 nb), which is larger than that in $^{26}\text{Mg} + ^{228}\text{Th}$ reaction. This is because the CN formed by the $^{26}\text{Mg} + ^{230}\text{Th}$ reaction has more neutrons, which easily decay via the $3n$ and $4n$ evaporation channels. Another reason is that the CN with smaller neutrons has a lower fission barrier height leading to a smaller survival probability.

The evaporation residue cross sections for $^{18}\text{O} + ^{242,244}\text{Pu}$ and $^{22}\text{O} + ^{242,244}\text{Pu}$ are shown in Fig. 7. The values of mass asymmetry of $^{18}\text{O} + ^{242}\text{Pu}$, $^{18}\text{O} + ^{244}\text{Pu}$, $^{22}\text{O} + ^{242}\text{Pu}$, and $^{22}\text{O} + ^{244}\text{Pu}$ are 0.94, 0.86, 0.83, and 0.84, respectively, which are larger than those of the $^{26}\text{Mg} + ^{228,230}\text{Th}$ systems (about 0.80). This leads to the maximum evaporation residue cross sections for the $^{18}\text{O} + ^{242,244}\text{Pu}$ and $^{22}\text{O} + ^{242,244}\text{Pu}$ systems

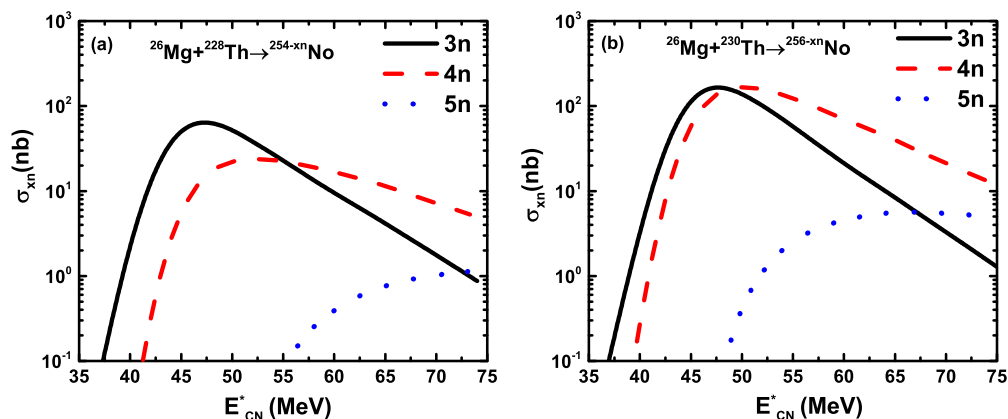


FIG. 6. (a) The calculated excitation functions for the xn -evaporation channels ($x = 2-5$) for the (a) $^{26}\text{Mg} + ^{228}\text{Th}$ and (b) $^{26}\text{Mg} + ^{230}\text{Th}$ reactions. The solid, dashed, dotted, and dash-dotted lines indicate the calculated results of the $3n$, $4n$, and $5n$ channels, respectively.

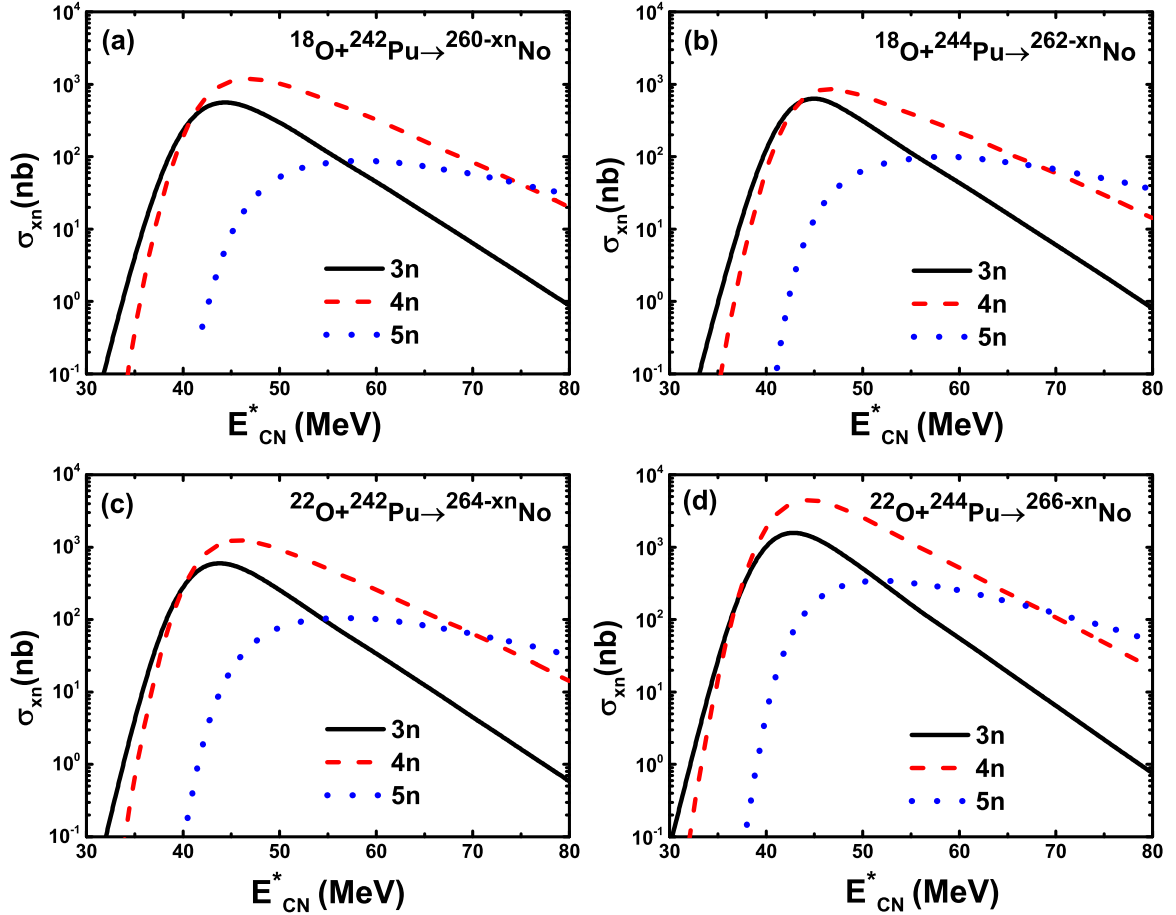


FIG. 7. (a) The calculated (lines) excitation functions for the xn -evaporation channels ($x = 3-5$) for the (a) $^{18}\text{O} + ^{242}\text{Pu}$, (b) $^{18}\text{O} + ^{244}\text{Pu}$, (c) $^{22}\text{O} + ^{242}\text{Pu}$, and (d) $^{22}\text{O} + ^{244}\text{Pu}$ reactions. The solid, dashed, and dotted lines indicate the calculated results of the $3n$, $4n$, and $5n$ channels, respectively.

($\sim 10^3$ nb) being significantly higher than those for the $^{26}\text{Mg} + ^{228,230}\text{Th}$ systems ($\sim 10^2$ nb). One can see that the peak value of the $4n$ emission channel in each panel is higher than that of the $3n$ channel. The survival probabilities of the $4n$ channel at $E^* = V_b + Q$ are larger compared to those of the $3n$ channel (see Fig. 4). The peak values of the $4n$ channel for the $^{18}\text{O} + ^{242}\text{Pu}$, $^{18}\text{O} + ^{244}\text{Pu}$, and $^{22}\text{O} + ^{242}\text{Pu}$ systems are 586.2, 487.1, and 628.1 nb, respectively. Because the combination of the neutron-rich projectile and the target has a larger capture cross section [see Fig. 3 (a)] and higher survival probability (see Fig. 4), the maximum value of σ_{4n} in the $^{22}\text{O} + ^{244}\text{Pu}$ reaction has reached 4649.3 nb.

C. A summary on the synthesis of No isotopes

The evaporation residue cross sections of No isotopes via different reactions at corresponding incident energies are given in Table II. For the $^{48}\text{Ca} + ^{204,206,207,208}\text{Pb}$, $^{12}\text{C} + ^{244,246,248}\text{Cm}$, and $^{13}\text{C} + ^{244,246,248}\text{Cm}$ reactions (with experimental data), the incident energies we take are consistent with the experimental data. For the reactions (like $^{26}\text{Mg} + ^{228,230}\text{Th}$, $^{18}\text{O} + ^{242,244}\text{Pu}$, and $^{22}\text{O} + ^{242,244}\text{Pu}$) without experimental data, we consider that the optimal incident energies in the

laboratory frame corresponds to the maximum cross sections. It can be seen that the experimental data are well reproduced (see Table II). One finds that both neutron-deficient ^{249}No and neutron-rich $^{261-263}\text{No}$ are synthesized by FE reactions. We predict the evaporation residue cross section of the reaction $^{26}\text{Mg} + ^{228}\text{Th}$ to be 1.2 nb for the $5n$ channel and the optimal excitation energy for the $5n$ channel is 74 MeV [see Fig. 6(a)].

The fusion of heavy ^{48}Ca nuclei with $^{204,206,207,208}\text{Pb}$ targets at near-barrier incident energies generates low-excited superheavy CN; in this case, one or two neutrons are more favorable to being evaporated. The fusion of these reactions use a cold-fusion mechanism in which neutron-deficient heavy nuclei are produced. It is noticed that $^{250-254}\text{No}$ are synthesized within the cold-fusion mechanism by $^{204}\text{Pb}(^{48}\text{Ca}, 2n)^{250}\text{No}$, $^{206}\text{Pb}(^{48}\text{Ca}, 3n)^{251}\text{No}$, $^{206}\text{Pb}(^{48}\text{Ca}, 2n)^{252}\text{No}$, $^{207}\text{Pb}(^{48}\text{Ca}, 2n)^{253}\text{No}$, and $^{208}\text{Pb}(^{48}\text{Ca}, 2n)^{254}\text{No}$ reactions in experiment and the evaporation residue cross sections are $13.2_{-6.7}^{+4.0}$, 30_{-7}^{+9} , 515_{-47}^{+80} , 1310_{-410}^{+430} , and 2050_{-340}^{+460} nb, respectively.

The fusion of $^{12,13}\text{C}$, ^{26}Mg , and $^{18,22}\text{O}$ with actinide targets ($^{228,230}\text{Th}$, $^{244,246,248}\text{Cm}$, and $^{242,244}\text{Pu}$) leads to the formation of quite-high-excitation-energy superheavy CN. In general, when the excitation energy is larger than 30 MeV,

TABLE II. The production cross sections of $^{249-263}\text{No}$ isotopes in FE reactions. The mass number and half-lives of these isotopes are tabulated in columns 1 and 2. The corresponding reactions, the incident energy in the laboratory frame E_{lab} , and the excitation energy E^* are listed in columns 3–5. The experimental values of the evaporation residue cross sections σ_{exp} in column 6 are taken from Refs. [11,51]. The calculated results are shown in the last column. For the reactions without experimental data, the calculated cross sections are the value.

Mass number	Half-life	Reaction	E_{lab} (MeV)	E^* (MeV)	σ_{exp} (nb)	σ_{cal} (nb)
249	—	$^{228}\text{Th}(^{26}\text{Mg}, 5n)$	164.9	74.0	—	1.2
250	$4.2_{-9}^{+12} \mu\text{s}$	$^{204}\text{Pb}(^{48}\text{Ca}, 2n)$	216.7	23.2	$13.2_{-6.7}^{+10.1}$	17.2
		$^{206}\text{Pb}(^{48}\text{Ca}, 4n)$	242.4	43.9	$0.26_{-0.13}^{+0.19}$	2.0
		$^{228}\text{Th}(^{26}\text{Mg}, 4n)$	140.4	52.0	—	23.9
251	$0.8 \pm 1 \text{ s}$	$^{206}\text{Pb}(^{48}\text{Ca}, 3n)$	226.2	30.7	30_{-7}^{+9}	44.2
		$^{244}\text{Cm}(^{12}\text{C}, 5n)$	83.0	49.7	90	8.3
252	$2.47 \pm 2 \text{ s}$	$^{206}\text{Pb}(^{48}\text{Ca}, 2n)$	217.1	23.3	515_{-47}^{+80}	168.4
		$^{230}\text{Th}(^{26}\text{Mg}, 4n)$	135.8	48.8	—	169.6
		$^{244}\text{Cm}(^{12}\text{C}, 4n)$	73.3	40.6	250	490.7
253	$1.62 \pm 15 \text{ min}$	$^{206}\text{Pb}(^{48}\text{Ca}, 1n)$	217.4	23.6	58_{-17}^{+16}	32.9
		$^{207}\text{Pb}(^{48}\text{Ca}, 2n)$	216.7	22.4	1310_{-410}^{+430}	2343.7
		$^{230}\text{Th}(^{26}\text{Mg}, 3n)$	133.6	47.0	—	172.4
		$^{244}\text{Cm}(^{13}\text{C}, 4n)$	72.8	40.5	300	219.6
		$^{246}\text{Cm}(^{12}\text{C}, 5n)$	83.0	50.3	240	49.6
254	$51 \pm 10 \text{ s}$	$^{208}\text{Pb}(^{48}\text{Ca}, 2n)$	216.7	22.3	2050_{-340}^{+460}	1604.7
		$^{244}\text{Cm}(^{13}\text{C}, 3n)$	69.8	37.7	120	445.7
		$^{246}\text{Cm}(^{12}\text{C}, 4n)$	72.0	39.9	1000	3510.2
		$^{246}\text{Cm}(^{13}\text{C}, 5n)$	78.5	46.6	560	169.0
255	$3.52 \pm 21 \text{ min}$	$^{242}\text{Pu}(^{18}\text{O}, 5n)$	106.8	58.0	—	88.3
		$^{246}\text{Cm}(^{13}\text{C}, 4n)$	69.5	38.0	620	444.6
		$^{248}\text{Cm}(^{12}\text{C}, 5n)$	77.8	46.3	580	27.2
256	$2.91 \pm 5 \text{ s}$	$^{242}\text{Pu}(^{18}\text{O}, 4n)$	93.9	46.0	—	1212.0
		$^{246}\text{Cm}(^{13}\text{C}, 3n)$	67.5	36.1	70	62.3
		$^{248}\text{Cm}(^{12}\text{C}, 4n)$	71.2	39.9	1000	1686.5
		$^{248}\text{Cm}(^{13}\text{C}, 5n)$	74.8	43.5	660	67.2
257	$25 \pm 3 \text{ s}$	$^{242}\text{Pu}(^{18}\text{O}, 3n)$	91.8	44.0	—	586.2
		$^{244}\text{Pu}(^{18}\text{O}, 5n)$	105.8	58.0	—	100.0
		$^{248}\text{Cm}(^{12}\text{C}, 3n)$	69.2	38.0	160	1884.8
		$^{248}\text{Cm}(^{13}\text{C}, 4n)$	70.5	39.4	1100	613.0
258	$1.2 \pm 2 \text{ s}$	$^{244}\text{Pu}(^{18}\text{O}, 4n)$	95.0	48.0	—	706.6
		$^{248}\text{Cm}(^{13}\text{C}, 3n)$	71.1	40.0	—	3526.1
259	$58 \pm 5 \text{ ms}$	$^{242}\text{Pu}(^{22}\text{O}, 5n)$	106.9	58.0	—	105.7
		$^{244}\text{Pu}(^{18}\text{O}, 3n)$	90.7	44.0	—	487.1
260	$106 \pm 8 \text{ ms}$	$^{242}\text{Pu}(^{22}\text{O}, 4n)$	93.8	46.0	—	1277.6
261	—	$^{242}\text{Pu}(^{22}\text{O}, 3n)$	91.6	44.0	—	628.1
		$^{244}\text{Pu}(^{22}\text{O}, 5n)$	100.8	52.0	—	346.9
262	—	$^{244}\text{Pu}(^{22}\text{O}, 4n)$	92.1	44.0	—	4649.3
263	—	$^{244}\text{Pu}(^{22}\text{O}, 3n)$	89.9	42.0	—	1638.2

in order to obtain a ground-state superheavy nuclei, there must be at least three neutrons to be evaporated. Reactions like these are called hot fusion. For the hot-fusion mechanism, the evaporation residue cross sections in the $3n$ and $4n$ evaporation channels are significantly large.

Note that more neutron-rich $^{257-263}\text{No}$ isotopes are synthesized via the hot-fusion reactions $^{242}\text{Pu}(^{18}\text{O}, 3n)^{257}\text{No}$, $^{248}\text{Cm}(^{13}\text{C}, 3n)^{258}\text{No}$, $^{244}\text{Pu}(^{18}\text{O}, 3n)^{259}\text{No}$, $^{242}\text{Pu}(^{22}\text{O}, 4n)^{260}\text{No}$, $^{242}\text{Pu}(^{22}\text{O}, 3n)^{261}\text{No}$, $^{244}\text{Pu}(^{22}\text{O}, 4n)^{262}\text{No}$, and $^{244}\text{Pu}(^{22}\text{O}, 3n)^{263}\text{No}$, respectively, with extremely large cross sections (see

Table II). The choice of the best exit channel depends on the choice of projectile-target combination and incident energy, which requires further exploration.

IV. CONCLUSIONS

The synthesis of No isotopes ($^{249-263}\text{No}$) are studied in FE reactions based on the DNS model. The three processes (capture, fusion, and survival) in the complete fusion reaction are investigated via the $^{18}\text{O} + ^{242}\text{Pu}$ and $^{22}\text{O} + ^{244}\text{Pu}$ reactions. It is shown that the capture process between the projectile and the target is dominated by the quantum tunneling effect in the case of the E^* of the system lower than $V_b + Q$. The reaction system with a larger mass asymmetry has a larger fusion probability. The CN with a larger neutron excess has a larger survival probability due to the higher fission barrier. The evaporation residue cross sections in the $^{48}\text{Ca} + ^{208}\text{Pb}$,

$^{26}\text{Mg} + ^{228,230}\text{Th}$, and $^{18,22}\text{O} + ^{242,244}\text{Pu}$ reactions have been studied and we find that, to obtain the new neutron-rich No isotopes ($^{261-263}\text{No}$), the radioactive beam as projectile and neutron-rich actinide as target should be chosen. The maximum evaporation residue cross sections of the $^{257-263}\text{No}$ isotopes calculated by the DNS model are 0.586, 3.526, 0.487, 1.277, 0.628, 4.649, and 1.638 μb , respectively.

ACKNOWLEDGMENTS

This work was supported by the National Natural Science Foundation of China under Grants No. 11635003, No. 11025524, and No. 11161130520; the National Basic Research Program of China under Grant No. 2010CB832903; and the European Commission's 7th Framework Programme (Fp7-PEOPLE-2010-IRSES) under Grant No. 269131.

-
- [1] Y. T. Oganessian *et al.*, *Phys. Rev. C* **69**, 054607 (2004).
 [2] K. Morita, K. Morimoto, D. Kaji, T. Akiyama, S. Goto, H. Haba, E. Ideguchi, R. Kanungo, K. Katori, H. Koura, H. Kudo, T. Ohnishi, A. Ozawa, T. Suda, K. Sueki, H. S. Xu, T. Yamaguchi, A. Yoneda, A. Yoshida, and Y. L. Zhao, *J. Phys. Soc. Jpn.* **73**, 2593 (2004).
 [3] Y. T. Oganessian *et al.*, *Phys. Rev. C* **76**, 011601(R) (2007).
 [4] P. A. Ellison, K. E. Gregorich, J. S. Berryman, D. L. Bleuel, R. M. Clark, I. Dragojević, J. Dvorak, P. Fallon, C. Fineman-Sotomayor, J. M. Gates, O. R. Gothe, I. Y. Lee, W. D. Loveland, J. P. McLaughlin, S. Paschalis, M. Petri, J. Qian, L. Stavsetra, M. Wiedeking, and H. Nitsche, *Phys. Rev. Lett.* **105**, 182701 (2010).
 [5] Y. T. Oganessian *et al.*, *Phys. Rev. C* **69**, 021601(R) (2004).
 [6] Y. T. Oganessian *et al.*, *Phys. Rev. C* **70**, 064609 (2004).
 [7] Y. T. Oganessian *et al.*, *Phys. Rev. Lett.* **104**, 142502 (2010).
 [8] Y. T. Oganessian *et al.*, *Phys. Rev. C* **74**, 044602 (2006).
 [9] E. D. Donets, V. A. Shchegolev, and V. A. Ermakov, *At. Energ.* **20**, 257 (1966).
 [10] B. A. Zager, M. B. Miller, V. L. Mikheev, S. M. Polikanov, A. M. Sukhov, G. N. Flerov, and L. P. Chelnokov, *At. Energ.* **20**, 264 (1966).
 [11] Y. T. Oganessian, V. K. Utyonkov, Y. V. Lobanov, F. S. Abdullin, A. N. Polyakov, I. V. Shirokovsky, Y. S. Tsyganov, A. N. Mezentsev, S. Iliev, V. G. Subbotin, A. M. Sukhov, K. Subotic, O. V. Ivanov, A. N. Voinov, V. I. Zagrebaev, K. J. Moody, J. F. Wild, N. J. Stoyer, M. A. Stoyer, and R. W. Loughheed, *Phys. Rev. C* **64**, 054606 (2001).
 [12] A. Ghiorso, T. Sikkeland, and M. J. Nurmi, *Phys. Rev. Lett.* **18**, 401 (1967).
 [13] V. L. Mikheev, V. I. Ilyushchenko, M. B. Miller, S. M. Polikanov, G. N. Flerov and Y. P. Kharitonov, *At. Energ.* **22**, 93 (1967).
 [14] V. A. Druin, G. N. Akap'ev, A. G. Demin, Y. V. Lobanov, B. V. Fefilov, G. N. Flerov, and L. P. Chelnokov, *At. Energ.* **22**, 135 (1967).
 [15] E. D. Donets, V. A. Shchegolets, and V. A. Ermakov, *At. Energ.* **16**, 233 (1964).
 [16] E. K. Hulet, J. F. Wild, R. J. Dougan, R. W. Loughheed, J. H. Landrum, A. D. Dougan, P. A. Baisden, C. M. Henderson, R. J. Dupzyk, R. L. Hahn, M. Schadel, K. Summerer, and G. R. Bethune, *Phys. Rev. C* **40**, 770 (1989).
 [17] R. J. Silva, P. F. Dittner, M. L. Mallory, O. L. Keller, K. Eskola, P. Eskola, M. Nurmi, and A. Ghiorso, *Nucl. Phys. A* **216**, 97 (1973).
 [18] L. P. Somerville, M. J. Nurmi, J. M. Nitschke, A. Ghiorso, E. K. Hulet, and R. W. Loughheed, *Phys. Rev. C* **31**, 1801 (1985).
 [19] M. Thoennessen, *The Discovery of Isotopes* (Springer, Switzerland, 2016).
 [20] K. E. Zyranski, W. Loveland, G. A. Souliotis, D. J. Morrissey, C. F. Powell, O. Batenkov, K. Aleklett, R. Yanez, and I. Forsberg, *Phys. Rev. C* **63**, 024615 (2001).
 [21] W. Loveland, D. Peterson, A. M. Vinodkumar, P. H. Sprunger, D. Shapira, J. F. Liang, G. A. Souliotis, D. J. Morrissey, and P. Lofy, *Phys. Rev. C* **74**, 044607 (2006).
 [22] J. F. Liang, D. Shapira, C. J. Gross, J. R. Beene, J. D. Bierman, A. Galindo-Uribarri, J. Gomez del Campo, P. A. Hausladen, Y. Larochele, W. Loveland, P. E. Mueller, D. Peterson, D. C. Radford, D. W. Stracener, and R. L. Varner, *Phys. Rev. Lett.* **91**, 152701 (2003).
 [23] C. Li, F. Zhang, J. J. Li, L. Zhu, J. L. Tian, N. Wang, and F. S. Zhang, *Phys. Rev. C* **93**, 014618 (2016).
 [24] A. S. Umar, V. E. Oberacker, and J. A. Maruhn, *Eur. Phys. J. A* **37**, 245 (2008).
 [25] C. W. Shen, Y. Abe, D. Boilley, G. Kosenko, and E. G. Zhao, *Int. J. Mod. Phys. E* **17**, 66 (2008).
 [26] G. G. Adamian, N. V. Antonenko, W. Scheid, and V. V. Volkov, *Nucl. Phys. A* **633**, 409 (1998).
 [27] Z. H. Liu and J. D. Bao, *Phys. Rev. C* **80**, 054608 (2009).
 [28] K. Siwek-Wilczynska, T. Cap, and J. Wilczynski, *Int. J. Mod. Phys. E* **19**, 500 (2010).
 [29] V. I. Zagrebaev, *Phys. Rev. C* **64**, 034606 (2001).
 [30] V. I. Zagrebaev and W. Greiner, *Phys. Rev. C* **78**, 034610 (2008).
 [31] V. I. Zagrebaev, A. V. Karpov, and W. Greiner, *Phys. Rev. C* **85**, 014608 (2012).
 [32] G. G. Adamian, N. V. Antonenko, S. P. Ivanova, and W. Scheid, *Nucl. Phys. A* **646**, 29 (1999).
 [33] G. G. Adamian, N. V. Antonenko, and W. Scheid, *Nucl. Phys. A* **678**, 24 (2000).
 [34] G. G. Adamian, N. V. Antonenko, W. Scheid, and V. V. Volkov, *Nucl. Phys. A* **627**, 361 (1997).
 [35] G. G. Adamian, N. V. Antonenko, and W. Scheid, *Nucl. Phys. A* **618**, 176 (1997).

- [36] K. H. Schmidt and W. Morawek, *Rep. Prog. Phys.* **54**, 949 (1991).
- [37] Z. Q. Feng, G. M. Jin, and J. Q. Li, *Phys. Rev. C* **80**, 057601 (2009).
- [38] P. Grangé, L. Jun-Qing, and H. A. Weidenmüller, *Phys. Rev. C* **27**, 2063 (1983).
- [39] G. G. Adamian, N. V. Antonenko, and W. Scheid, *Phys. Rev. C* **68**, 034601 (2003).
- [40] C. Y. Wong, *Phys. Rev. Lett.* **31**, 766 (1973).
- [41] Z. Q. Feng, G. M. Jin, J. Q. Li, and W. Scheid, *Phys. Rev. C* **76**, 044606 (2007).
- [42] J. Q. Li and G. Wolschin, *Phys. Rev. C* **27**, 590 (1983).
- [43] W. Reisdorf, *Z. Phys. A* **300**, 227 (1981).
- [44] W. Reisdorf and M. Schädel, *Z. Phys. A* **343**, 47 (1992).
- [45] R. J. Charity, M. A. McMahan, G. J. Wozniak, R. J. McDonald, L. G. Moretto, D. G. Sarantites, L. G. Sobotka, G. Guarino, A. Pantaleo, L. Fiore, A. Gobbi, and K. D. Hildenbrand, *Nucl. Phys. A* **483**, 371 (1988).
- [46] V. Weisskopf, *Phys. Rev.* **52**, 295 (1937).
- [47] N. Bohr and J. A. Wheeler, *Phys. Rev.* **56**, 426 (1939).
- [48] A. S. Zubov, G. G. Adamian, N. V. Antonenko, S. P. Ivanova, and W. Scheid, *Phys. Rev. C* **65**, 024308 (2002).
- [49] J. D. Jackson, *Can. J. Phys.* **34**, 767 (1956).
- [50] E. A. Cherepanov, A. S. Ijginov, and M. V. Mebel, *J. Phys. G* **9**, 931 (1983).
- [51] T. Sikkeland, A. Ghiorso, and M. J. Nurmi, *Phys. Rev.* **172**, 1232 (1968).